JOURNAL OF SPACECRAFT AND ROCKETS
Vol. 47, No. 1, January–February 2010

Fully Structured Aerodynamic Model for Parameter Identification of a Reentry Experimental Vehicle

Nicola de Divitiis*
University of Rome "La Sapienza," 00184 Rome, Italy
and
Antonio Vitale†
Italian Aerospace Research Centre, 81043 Capua, Italy

DOI: 10.2514/1.45304

Vehicle preflight aerodynamic databases are frequently validated and improved using system identification techniques that require the availability of flight data and the definition of suitable aerodynamic models. In this framework, the paper presents a novel theoretical aerodynamic model to be used for the aerodynamic identification of a lifting body in subsonic, transonic, and supersonic regimes. The proposed model is based on the general properties of the continuity equation in the von Kármán form. Each aerodynamic coefficient incorporates free parameters to be estimated from the flight data analysis and takes into account the simultaneous effects of the several vehicle state variables. The proposed model was applied to the identification from the flight data of an experimental vehicle of the Italian Aerospace Research Centre. Identification results show that the model is able to perform an excellent fitting of the aerodynamic coefficients experimented in flight by the vehicle.

Nomenclature

$\mathbf{A}$, $\mathbf{B}$	=	influence matrices
b	=	wing span, m
C_D, C_S, C_L	=	aerodynamic force coefficients in wind axes
C_l, C_m, C_n	=	aerodynamic moment coefficients in body axes
C_X, C_Y, C_Z	=	aerodynamic force coefficients in body axes
c	=	mean chord, m
$\mathbf{F}$	=	aerodynamic force in body axes (X, Y, and Z), N
F_{hk}	=	characteristic static function
G_{hk}	=	characteristic rotational function
L	=	vehicle reference length, m
$\mathbf{L}_{BW}$	=	transformation matrix from wind to body frames
$\mathbf{M}$	=	aerodynamic moment in body axes (L, M, and N), N · m
M_∞	=	flight Mach number
$\mathbf{n}$	=	normal unit vector to the wetted surface
n_x, n_z	=	longitudinal and normal components of the acceleration in body axes, m/s^2
P	=	local air pressure, N/m^2
$\mathbf{r}_{\text{c.g.}}$	=	vehicle center of gravity location, m
S	=	vehicle reference surface, m^2
S_w	=	vehicle wetted surface, m^2
x, y, z	=	body axes coordinate, m
$\tilde{x}$, $\tilde{y}$, $\tilde{z}$	=	wind axes coordinate, m
$\mathbf{V}$	=	flight velocity in body axes (u, v, and w), m/s
V	=	flight speed, m/s
$\hat{\mathbf{V}}$	=	flight velocity unit vector in body axes ($\hat{u}$, $\hat{v}$, and $\hat{w}$)
V_∞	=	stream velocity (V), m/s
$\mathbf{v}$	=	local fluid velocity in body axes, m/s
α	=	angle of attack, deg
β	=	sideslip angle, deg
γ	=	air specific heat ratio
δ_a, δ_e, and δ_r	=	ailerons, elevator, and rudder deflections, respectively, deg
ϕ	=	velocity potential, m^2/s
$\boldsymbol{\omega}$	=	angular velocity in body axes (p, q, r), deg /s

Received 5 May 2009; revision received 25 September 2009; accepted for publication 9 October 2009.

*Assistant Professor, Department of Mechanics and Aeronautics, Via Eudossiana 18.

†Research Engineer, Guidance, Navigation, and Control Laboratory, via Maiorise.

I. Introduction

THE present work is in the framework of the identification of the aerodynamic coefficients of a spacecraft through flight data analysis. To identify these coefficients, a physico-mathematical model, which incorporates several free parameters, is proposed.

Preflight aerodynamic databases, obtained by means of wind-tunnel tests and computational fluid dynamics analyses, are usually to be refined using test flight data and system identification techniques in order to reduce the level of uncertainty on aerodynamic coefficients. System identification from flight data calls for structured parametric aerodynamic models based on physical consideration and able to represent, with adequate accuracy, the flowfield characteristics in the regimes of interest. In fact, as a major advantage of such a structured model, the parameter values identified from the analysis of a single trajectory could be extended to a wide region of the flight envelope. This characteristic is relevant, especially if few flight tests specifically aimed at system identification can be performed, as usually happens for a reentry vehicle. On the other hand, the determination of the aerodynamic coefficients of the lifting-body configurations for reentry vehicles, in the diverse situations, is a very difficult task for various reasons.

The first of them is of a physical nature and arises from the variations of the flow structure about the aircraft, which depends on the current vehicle state variables and on some of their time derivatives (i.e., M_∞, α, β, p, q, r, $\mathrm{d}\alpha/\mathrm{d}t$, and $\mathrm{d}\beta/\mathrm{d}t$). The simultaneous effect of all these quantities produces a pressure distribution on the aircraft surface, which depends on such variables in a complex fashion [1]. Because of this complexity, the determination of reasonable expressions of the aerodynamic coefficients, in terms of the current state variables, can be very difficult. Although the aerodynamic performance of several lifting vehicles, such as HL-10, HL-20, X-33, and X-38, have only recently been analyzed [2,3], the development of a general method for calculating the aerodynamic characteristics in subsonic, transonic, and supersonic regimes for lifting bodies have not reached the same level of the classical

wing-body analysis, especially for what concerns the variations of the lateral and directional coefficients in terms of the aerodynamic angles and the flight Mach number [3–5]. In fact, the simultaneous effects of the lateral flow, spin rates, and the fluid compressibility can determine complex situations, for which these coefficients exhibit nontrivial nonmonotonic variations (with α for several M) [3].

The next reason is of a mathematical nature and regards the use of a tabular aerodynamic coefficient database. If the aerodynamic coefficients were known for assigned values of the state variables, the coefficient values elsewhere (calculated through an interpolation procedure) will give a result for which the accuracy depends on the adopted interpolation method and on the number of the arguments [6]. Because these coefficients depend on quite a great number of state variables, the interpolation provides (in general) poor accuracy [6], especially for the transonic variations of the lateral and directional coefficients at $\beta \neq 0$, $p \neq 0$, and $r \neq 0$.

Whereas the wind-tunnel tests and the computational fluid dynamics supply the measurement and the computation of the aerodynamic coefficients of the bodies of arbitrary shape, the theoretical aerodynamics mainly provide the analytical tools for the longitudinal aerodynamic coefficients of the wing and the fuselage [7–10]. As a result, the aforementioned difficulties are encountered (especially for the lateral-directional derivatives, such as the dihedral effect, yaw stiffness, or the rotational derivatives), whereas, because of the simultaneous effects, the modellation of these derivatives could require the consideration of the combined variations of M_∞, α, β, and spin rates.

Last, but not least, the aerodynamic controls, which influence the aerodynamic coefficients in conjunction with all the variables, determine a further difficulty for the determination of the aerodynamic coefficients of a lifting body.

From the theoretical standpoint, one can obtain a good (or at least a reasonable) estimation of the aerodynamic coefficients if these latter are expressed through functions, which arise from the physical properties of the flow around the vehicle. This is the basic idea of the present paper, the main purpose of which is to suggest a novel physico-mathematical model to be used for the identification of the aerodynamic coefficients of a lifting body in subsonic, transonic, and supersonic regimes. The model, for which the incompressible version has just been proposed by the author in [11] for studying the aerodynamics of a shrouded-fan unmanned aerial vehicle (UAV), is based on a physical hypothesis about the flow around the obstacles. These conjectures arise from the Kirchoff theorem [1], which in origin was formulated for incompressible streams and is based on the linear property of the continuity equation. This theorem states that, for an incompressible flow, the local fluid velocity around an obstacle is a linear function of the peculiar velocities of the problem [1]. To study the vehicle aerodynamics in the compressible regimes, the Kirchoff theorem is properly extended here to the compressible streams, taking into account that the local velocity depends on the fluid compressibility through the von Kármán equation. The model allows one to analytically express each aerodynamic coefficient as a nonlinear function of Mach numbers, aerodynamic angles, control angles, angular rates, and a set of constant aerodynamic parameters to be properly identified.

The proposed model was applied to the aerodynamic model identification from the flight data of the flying test bed 1 (FTB_1) vehicle of the Italian Aerospace Research Centre (CIRA).

System identification was carried out in two steps. First, a preflight tabular aerodynamic database of FTB_1 (CIRA-ADB), developed by CIRA [12] and obtained by means of the wind-tunnel tests and computational fluid dynamics analyses, was used to preidentify all the aerodynamic parameters of the model. Then, a subset of such parameters (selected through identifiability analysis) was updated using the flight data of the first FTB_1 mission, called the dropped transonic flight test 1 ($DTFT_1$). The identified model is able to perform an excellent fitting of the aerodynamic coefficients experimented by the vehicle during the $DTFT_1$ mission. Moreover, a relevant reduction of the aerodynamic uncertainty with regard to the CIRA-ADB is obtained.

In what follows in Sec. II, the $DTFT_1$ mission profile is described, and Sec. III deals with the proposed aerodynamic model. Section IV is dedicated to the description of the identification procedure used to evaluate the model-free parameters. Next, identification results and discussion are presented in Sec. V, and a section of conclusions ends the paper.

II. Mission Profile

The CIRA is conducting an unmanned space vehicle (USV) program with the main objective of designing and manufacturing unmanned flying test beds (FTBs). The FTBs are multimission flying laboratories aimed at testing and verifying innovative materials, aerodynamic behavior, advanced guidance, navigation, and control functionalities (as well as the critical operational aspects peculiar to the future reusable launch vehicle [13]). FTB_1, the first vehicle of the USV program, is shown in Fig. 1, and its main characteristics are described in [12]. It is unmanned and unpowered, and it has been developed to perform flight missions for investigation of subsonic, transonic, and low supersonic regimes. The FTB_1 is a winged slender configuration with two sets of aerodynamic effectors: the elevons, which provide both pitch control when deflected symmetrically and roll control when deflected asymmetrically, and the rudders, which deflect only symmetrically to allow yaw control. Lateral-directional stability is enhanced by means of two ventral fins. The tabular database was used to preidentify all the aerodynamic parameters of the proposed analytical aerodynamic model. A subset of such parameters, selected through identifiability analysis, was updated using flight data of the first FTB_1 mission (named $DTFT_1$). The FTB_1 mission was executed in February 2007, and the main objective was to investigate the transonic flight of a reentry vehicle. The basic operations consisted of three main phases. First, an ascent phase was operated by a stratospheric balloon that brought the vehicle at the release altitude of about 20 km. Next, the flight phase followed, in which the FTB_1 left the carrier and started a free flight, accelerating to achieve a Mach number between 1 and 1.1 at an altitude between 10 and 15 km. Finally, in the deceleration phase, the FTB_1 opened the parachute and ended its mission by water splashdown. The $DTFT_1$ nominal mission profile is sketched in Figs. 2 and 3. The time interval considered for the aerodynamic model identification lasted 27 s, from the flight time (after the vehicle was dropped from the carrier) of $t = 17$ through 44 s. Time histories of the angle of attack and Mach number for that time frame are shown in Fig. 3. The Mach number varies from 0.57 to about 1.08, whereas the angle of attack was held nearly constant at about 7 deg (the reference angle of attack along the nominal trajectory) by the flight controls system (FCS) for 39 s. The transonic regime started at about $t = 31$ s, for which the displacement of the aerodynamic center determined a large perturbation on the pitch moment. At $t = 39$ s, due to a problem in the parachute opening at the beginning of the deceleration phase at about $h = 13,885$ m and $M = 1.04$, the FCS switched into a safety mode, as expected in this abnormal situation, because the constraint on the maximum allowable load factor was violated. As a result, the aerodynamic control surfaces were rapidly brought to the neutral position to determine the variations of α visible in the figure at $t > 39$ s and resulting from the strong excitation of the short period dynamic of the vehicle. In the entire flight, the vehicle trajectory was basically

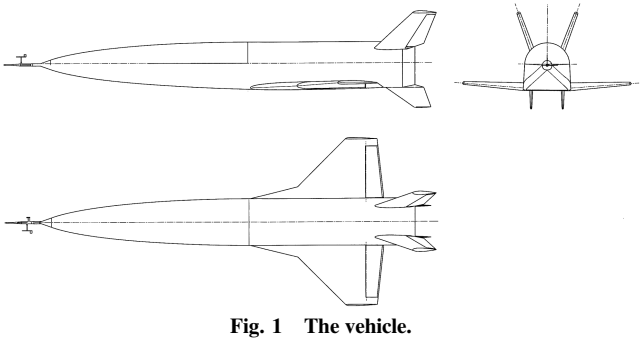

Fig. 1 The vehicle.

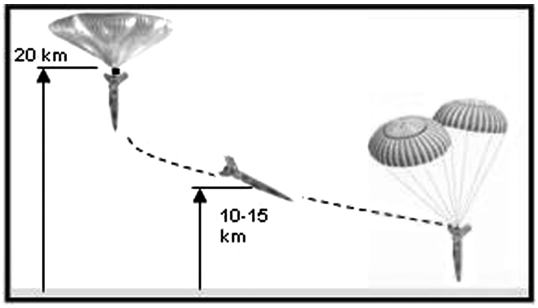

Fig. 2 $DFTF_1$ nominal mission profile.

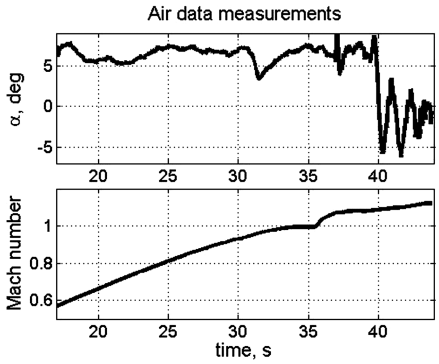

Fig. 3 Angle of attack and Mach number during $DFTF_1$.

longitudinal, with the sideslip angle accurately tracking the 0 deg reference value. Flight data acquired during the $DTFT_1$ mission were used to identify the FTB_1 vehicle aerodynamics.

III. Structured Aerodynamic Model for System Identification

In this section, the vehicle aerodynamics are analyzed with the continuity equation. The perturbed stream in the proximity of the aircraft is described with the local perturbed velocity, which in the wind frame is

$$\tilde{\mathbf{v}}(\mathbf{r}) \equiv (\tilde{u},\ \tilde{v},\ \tilde{w}) \tag{1}$$

where $\tilde{u}$, $\tilde{v}$, and $\tilde{w} \ll V_\infty$, thus

$$|\mathbf{v}| = \sqrt{(V_\infty + \tilde{u})^2 + \tilde{v}^2 + \tilde{w}^2} \simeq V_\infty + \tilde{u} \tag{2}$$

The component $\tilde{u}$ corresponds to the direction $\tilde{x}$ parallel to $\mathbf{V}$, whereas $\tilde{v}$ and $\tilde{w}$ are the lateral components of the perturbed velocity. In this situation, $\mathbf{v}$ satisfies the continuity equation, which, in the wind frame, is written as follows [7,8,10]:

$$B\frac{\partial \tilde{u}}{\partial \tilde{x}} + \frac{\partial \tilde{v}}{\partial \tilde{y}} + \frac{\partial \tilde{w}}{\partial \tilde{z}} = 0 \tag{3}$$

with

$$B = 1 - M_\infty^2[1 + \tilde{u}(1 + \gamma)]$$

where $\tilde{y}$ and $\tilde{z}$ are the normal coordinates to $\mathbf{V}$. This is the von Kármán equation, which is obtained under the hypothesis of small perturbations (i.e., for small α, β, and thickness). For a small enough M_∞, all the points around the aircraft are subsonic, $B > 0$ in any case, and Eq. (3) is an elliptical equation. On the contrary, when each point is supersonic, $B < 0$ everywhere and Eq. (3) is a hyperbolic equation. In both the cases, B can be approximated by the expression

$$B = 1 - M_\infty^2 \tag{4}$$

and Eq. (3) can be reduced to a linear equation for the local velocity, therefore $\mathbf{v}$ is a linear function of the characteristic velocities of the problem. This is an extension of the Kirchoff theorem [1], which is applied here to the compressible stream. With reference to Fig. 4, the characteristic velocities for a rigid vehicle moving in a fluid are $\mathbf{V}$ and $\boldsymbol{\omega}$, which are both written in body frame:

$$\mathbf{V} = V\hat{\mathbf{V}}, \qquad \hat{\mathbf{V}} = \begin{bmatrix} \hat{u} \\ \hat{v} \\ \hat{w} \end{bmatrix} \equiv \begin{bmatrix} \cos\alpha\cos\beta \\ \sin\beta \\ \sin\alpha\cos\beta \end{bmatrix}, \qquad \boldsymbol{\omega} = \begin{bmatrix} p \\ q \\ r \end{bmatrix} \tag{5}$$

where $\hat{u}$,$\hat{v}$, and $\hat{w}$ are the direction cosines of $\mathbf{V}$ in the body frame. Thus, the local fluid velocity is

$$\mathbf{v}(\mathbf{r}) = \mathbf{A}(\mathbf{r},\ M_\infty)\mathbf{V} + \mathbf{B}(\mathbf{r},\ M_\infty)\boldsymbol{\omega} \tag{6}$$

This expresses the Kirchoff theorem applied to the von Kármán equation, where $\mathbf{A} = \partial\mathbf{v}/\partial\mathbf{V}$ and $\mathbf{B} = \partial\mathbf{v}/\partial\boldsymbol{\omega}$ are the Jacobian matrices of $\mathbf{v}$ with respect to $\mathbf{V}$ and $\boldsymbol{\omega}$, respectively. These derivatives are the influence functions that, for $M < 1$ or for $M > 1$, only depend on M_∞ and $\mathbf{r}$.

In the transonic regime, the nonlinear term of Eq. (3) is nonnegligible with regard to the others, and the von Kármán equation is locally elliptic or hyperbolic, following the sign of B. As a result, the influence functions will also depend on $\mathbf{V}$ and $\boldsymbol{\omega}$. The solutions of Eq. (3) are formally expressed by the continuation method in the form of [14]:

$$\mathbf{v}(\mathbf{r}) = \int_0^{\mathbf{V}} \frac{\partial \mathbf{v}}{\partial \mathbf{V}}(\mathbf{r},\ M_\infty,\ \mathbf{V},\ \boldsymbol{\omega})\,\mathrm{d}\mathbf{V} + \int_0^{\omega} \frac{\partial \mathbf{v}}{\partial \boldsymbol{\omega}}(\mathbf{r},\ M_\infty,\ \mathbf{V},\ \boldsymbol{\omega})\,\mathrm{d}\boldsymbol{\omega} \tag{7}$$

This velocity, which accounts for the variations of the flow structure about the aircraft, depends on the path integrals of Eq. (7), which are described by the time histories of $\mathbf{V}$ and $\boldsymbol{\omega}$ [14]. For steady-state aerodynamics, the local fluid velocity depends on the current state variables, thus Eq. (7) reads as follows:

$$\mathbf{v}(\mathbf{r}) = \mathbf{A}(\mathbf{r},\ M_\infty,\ \mathbf{V},\ \boldsymbol{\omega})\mathbf{V} + \mathbf{B}(\mathbf{r},\ M_\infty,\ \mathbf{V},\ \boldsymbol{\omega})\boldsymbol{\omega} \tag{8}$$

According to Eq. (3), $\mathbf{A}$ and $\mathbf{B}$ are almost independent from $\mathbf{V}$ and $\boldsymbol{\omega}$ for $M_\infty \ll 1$ or $M_\infty \gg 1$, whereas they are not for $M_\infty \approx 1$ because of the presence of the nonlinear term in Eq. (3).

It is worthy of remark that this analysis only holds if the variations of the flow structure around the vehicle are considered to be known when α, β, and $\boldsymbol{\omega}$ change. The flow structure is supposed to be assigned, and this implies that the solutions of Eq. (3) do not modify their analytical forms with respect to Eq. (8).

A. Steady Aerodynamic Coefficients

The present section deals with the calculation of the steady aerodynamic coefficients for the vehicle. The influence of the Reynolds number on the aerodynamic coefficients is not taken into account here.

Because $|\mathbf{v}|$ is almost expressed by its longitudinal component $\tilde{u}$ for thin bodies, which in turn depends on the components of $\mathbf{V}$ in the body axes, the aerodynamic force coefficients in the body frame exhibit more oscillating variations with regard to α than those in the

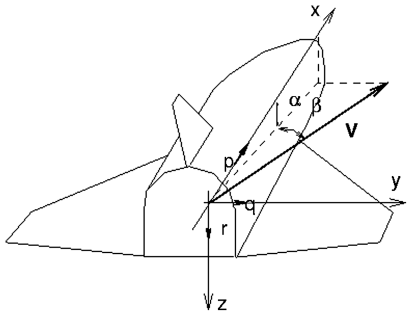

Fig. 4 Characteristic velocities and reference frame.

wind axes. This is due to the transformation matrix $\mathbf{L}_{WB}$, which determines more rapid variations as α and β change [1]. On the contrary, the moment coefficients exhibit quite smooth variations in body axes [1]. For this reason, the aerodynamic force and moment are calculated in the wind frame and body axes, respectively. The force and moment are expressed through the corresponding aerodynamic coefficients:

$$\mathbf{F} = -\frac{1}{2}\rho V^2 S \begin{bmatrix} C_D \\ C_S \\ C_L \end{bmatrix}; \qquad \mathbf{M} = \frac{1}{2}\rho V^2 S L \begin{bmatrix} C_l \\ C_m \\ C_n \end{bmatrix} \tag{9}$$

where L is the vehicle characteristic length. Then, the aerodynamic force coefficients in the body frame will be obtained through $\mathbf{L}_{WB}$.

The flow velocity around the vehicle varies according to Eq. (8), which is here expressed as

$$\mathbf{v}(\mathbf{r}) = V\left(\mathbf{A}\hat{\mathbf{V}} + \frac{1}{L}\mathbf{B}\hat{\boldsymbol{\omega}}\right) \tag{10}$$

where $\hat{\boldsymbol{\omega}} = \boldsymbol{\omega} L/V$ is the dimensionless angular velocity.

Hence, the aerodynamic force and moment are calculated as surface integrals of the pressure P over the vehicle wetted surface:

$$\mathbf{F} = -\int_{S_w} P\mathbf{n}\,\mathrm{d}S, \qquad \mathbf{M} = -\int_{S_w} P(\mathbf{r} - \mathbf{r}_{\mathrm{c.g.}}) \times \mathbf{n}\,\mathrm{d}S \tag{11}$$

where P is determined with the steady Bernoulli theorem, in which the square of $\mathbf{v}$ is expressed with Eq. (8):

$$\mathbf{v}\cdot\mathbf{v} \equiv v^2(\mathbf{r}) = V^2 \sum_{i=1}^{3}\sum_{j=1}^{3}\sum_{k=1}^{3}\{A_{ij}A_{ik}\hat{v}_j\hat{v}_k + A_{ij}B_{ik}\hat{v}_j\hat{\omega}_k + B_{ij}B_{ik}\hat{\omega}_j\hat{\omega}_k\} \tag{12}$$

The contribution of the skin friction does not appear in Eqs. (11), and its effect is considered to be caused by a proper pressure reduction [1,9]. Thus, the generic aerodynamic coefficient C_i ($i = D, S, L, l, m$, and n) is

$$C_i(\alpha, \beta, p, q, r) = \sum_{h=1}^{3}\sum_{k=1}^{3}\{F^i_{hk}\hat{v}_h\hat{v}_k + G^i_{hk}\hat{v}_h\hat{\omega}_k + H^i_{hk}\hat{\omega}_h\hat{\omega}_k\} \tag{13}$$

where $(\hat{v}_1, \hat{v}_2, \hat{v}_3) \equiv (\hat{u}, \hat{v}, \hat{w})$, $(\hat{\omega}_1, \hat{\omega}_2, \hat{\omega}_3) \equiv (\hat{p}, \hat{q}, \hat{r})$, although F^i_{hk}, G^i_{hk}, and H^i_{hk} are surface integrals of the functions of $\mathbf{r}$:

$$\sum_{i=1}^{3} A_{ih}A_{ik}$$

$$\sum_{i=1}^{3} A_{ih}B_{ik}$$

and

$$\sum_{i=1}^{3} B_{ih}B_{ik}$$

over S_w. Although $\mathbf{A}$ and $\mathbf{B}$ are functions of $\mathbf{V}$ and $\boldsymbol{\omega}$, the quantities F^i_{hk}, G^i_{hk}, and H^i_{hk}, which represent the aerodynamic derivatives, vary with M_∞, although they exhibit quite small variations with α, β, and $\boldsymbol{\omega}$ for thin obstacles ([9,10] and references therein). Hence, according to the literature, these integrals are supposed to be functions of M_∞ alone. These integrals show rather smooth variations with respect to M_∞ in the subsonic and supersonic regions [9,10], whereas for $M_\infty \approx 1$, sizable variations, caused by the fluid transonic regime, are observed.

From Eq. (13), C_i incorporates three addends; the first addend is the static aerodynamic coefficient, whereas the second one, which provides the simultaneous effect of $\mathbf{V}$ and $\boldsymbol{\omega}$, represents the contribution of the rotational derivatives. The last term is a quadratic form of $\boldsymbol{\omega}$ that, in the aerospace applications, is negligible with respect to the others. Therefore, C_i is expressed as follows:

$$C_i(\alpha, \beta, p, q, r) = \sum_{h=1}^{3}\sum_{k=1}^{3}\{F^i_{hk}\hat{v}_h\hat{v}_k + G^i_{hk}\hat{v}_h\hat{\omega}_k\} \tag{14}$$

where F^i_{hk} and G^i_{hk} are functions of M_∞ and are (here) called static and rotational characteristic functions, respectively. These functions are the second-order derivatives of the generic aerodynamic coefficient with regard to the direction cosines of $\mathbf{V}$ and to the dimensionless angular velocity; that is,

$$F^i_{hk}(M_\infty) \equiv \frac{1}{2}\frac{\partial^2 C_i}{\partial\hat{v}_h\partial\hat{v}_k}, \qquad G^i_{hk}(M_\infty) \equiv \frac{\partial^2 C_i}{\partial\hat{v}_h\partial\hat{\omega}_k} \tag{15}$$

where, without lack of generality [1], it is assumed that $F^i_{hk} = F^i_{kh}$. These derivatives are functions of the Mach number, for which the structure is supposed to be

$$\mathcal{F}_k(M_\infty) = \mathcal{F}_{k0}H_{\mathrm{sub}}\frac{\sqrt{\varepsilon+m}(1 + h_1M_\infty^2 + h_2M_\infty^3)}{\sqrt{\varepsilon + m|1 - M_\infty^\xi|^2}} + \mathcal{F}_{k\,\mathrm{sup}}H_{\mathrm{sup}}\frac{1 + g_1M_\infty^{y_1}}{1 + g_2M_\infty^{y_2}} \tag{16}$$

This expression incorporates two addends; the first addend reproduces the variation of the aerodynamic coefficients in the subsonic regime, whereas the second one describes the supersonic region. The quantities H_{sub} and H_{sup} are two sigmoidal functions of M_∞, which are chosen as follows:

$$H_{\mathrm{sub}}(M_\infty) = \frac{\tanh h(1 - M_\infty) + 1}{2}; \quad H_{\mathrm{sup}}(M_\infty) = \frac{\tanh h(M_\infty - 1) + 1}{2} \tag{17}$$

For this choice, $H_{\mathrm{sub}} \approx 1$ and $H_{\mathrm{sup}} \approx 0$ for $M_\infty \ll 1$, whereas $H_{\mathrm{sub}} \approx 0$ and $H_{\mathrm{sup}} \approx 1$ in the supersonic regime. Thus, the two terms of Eq. (16) are independent each other, but for $M_\infty \approx 1$, for which their combination describes the variations of the aerodynamic coefficients in the transonic regime. The parameter h is a proper constant, which accounts for these variations in the transonic regime. In Eq. (16), $\mathcal{F}_{k0}$ denotes $\mathcal{F}_k$ at $M_\infty = 0$, whereas $\mathcal{F}_{k\,\mathrm{sup}}$ represents the variation law in the supersonic regime.

Equation (15) can be considered an extension of the Levi–Civita formula, which gives the analytical expression of the pressure drag that, in origin, was applied to the incompressible regime [1]. According to the Levi–Civita formula, the second-order derivatives of the drag coefficient with regard to $\hat{u}$, $\hat{v}$, and $\hat{w}$ do not depend on the direction of $\mathbf{V}$, whereas, in the present formulation, due to the fluid compressibility, these derivatives are functions of M_∞. There exists a link between these derivatives and those of the classical formulation, which is reported here by means of the following relationships (which are only valid for $\alpha = \beta = p = q = r = 0$). For the static coefficients, these derivatives are

$$\frac{\partial^2 C_i}{\partial\hat{u}^2} \equiv 2C_i, \qquad \frac{\partial^2 C_i}{\partial\hat{u}\partial\hat{v}} \equiv \frac{\partial C_i}{\partial\beta}, \qquad \frac{\partial^2 C_i}{\partial\hat{u}\partial\hat{w}} \equiv \frac{\partial C_i}{\partial\alpha}$$
$$\frac{\partial^2 C_i}{\partial\hat{v}^2} \equiv \frac{\partial^2 C_i}{\partial\beta^2}, \qquad \frac{\partial^2 C_i}{\partial\hat{v}\partial\hat{w}} \equiv \frac{\partial^2 C_i}{\partial\beta\partial\alpha}, \qquad \frac{\partial^2 C_i}{\partial\hat{w}^2} \equiv \frac{\partial^2 C_i}{\partial\alpha^2} \tag{18}$$

whereas the rotational derivatives are

$$\frac{\partial^2 C_i}{\partial\hat{u}\partial\hat{p}} \equiv \frac{\partial C_i}{\partial\hat{p}}, \qquad \frac{\partial^2 C_i}{\partial\hat{u}\partial\hat{q}} \equiv \frac{\partial C_i}{\partial\hat{q}}, \qquad \frac{\partial^2 C_i}{\partial\hat{u}\partial\hat{r}} \equiv \frac{\partial C_i}{\partial\hat{r}}$$
$$\frac{\partial^2 C_i}{\partial\hat{v}\partial\hat{p}} \equiv \frac{\partial^2 C_i}{\partial\beta\partial\hat{p}}, \qquad \frac{\partial^2 C_i}{\partial\hat{v}\partial\hat{q}} \equiv \frac{\partial^2 C_i}{\partial\beta\partial\hat{q}}, \qquad \frac{\partial^2 C_i}{\partial\hat{v}\partial\hat{r}} \equiv \frac{\partial^2 C_i}{\partial\beta\partial\hat{r}}$$
$$\frac{\partial^2 C_i}{\partial\hat{w}\partial\hat{p}} \equiv \frac{\partial^2 C_i}{\partial\alpha\partial\hat{p}}, \qquad \frac{\partial^2 C_i}{\partial\hat{w}\partial\hat{q}} \equiv \frac{\partial^2 C_i}{\partial\alpha\partial\hat{q}}, \qquad \frac{\partial^2 C_i}{\partial\hat{w}\partial\hat{r}} \equiv \frac{\partial^2 C_i}{\partial\alpha\partial\hat{r}} \tag{19}$$

Because (x, z) is the symmetry plane, each longitudinal aerodynamic coefficient, such as C_D, C_L, and C_m, is an even function of β and results in an odd function of the products $\hat{v}\,\hat{r}$ and $\hat{v}\,\hat{p}$, whereas the lateral-directional coefficients, such as C_S, C_l, and C_n, are odd functions of β and of the products $\hat{u}\,\hat{p}$, $\hat{u}\,\hat{r}$, $\hat{v}\,\hat{q}$, $\hat{w}\,\hat{p}$, and $\hat{w}\,\hat{r}$. In view of Eqs. (5), the aerodynamic force and moment coefficients are written in terms of the aerodynamic angles and of the angular velocity components.

The force coefficients, written in wind axes, are

$$\begin{aligned}
C_D &= (F^D_{uu}\cos^2\alpha + F^D_{uw}\cos\alpha\sin\alpha + F^D_{ww}\sin^2\alpha)\cos^2\beta + F^D_{vv}\sin^2\beta \\
&\quad + (G^D_{uq}\cos\alpha\cos\beta + G^D_{wq}\sin\alpha\cos\beta)\hat{q} + (G^D_{vr}\hat{r} + G^D_{vp}\hat{p})\sin\beta \\
C_S &= (F^S_{uv}\cos\alpha + F^S_{vw}\sin\alpha)\sin\beta\cos\beta + (G^S_{up}\hat{p} \\
&\quad + G^S_{ur}\hat{r})\cos\alpha\cos\beta + G^S_{vq}\sin\beta\hat{q} + (G^S_{wp}\hat{p} + G^S_{wr}\hat{r})\sin\alpha\cos\beta \\
C_L &= (F^L_{uu}\cos^2\alpha + F^L_{uw}\cos\alpha\sin\alpha + F^L_{ww}\sin^2\alpha)\cos^2\beta + F^L_{vv}\sin^2\beta \\
&\quad + (G^L_{uq}\cos\alpha\cos\beta + G^L_{wq}\sin\alpha\cos\beta)\hat{q} + (G^L_{vr}\hat{r} + G^L_{vp}\hat{p})\sin\beta
\end{aligned} \tag{20}$$

As seen, the aerodynamic force coefficients in the body frame will be obtained by means of C_D, C_S, and C_L through the transformation matrix $\mathbf{L}_{BW}$. The moment aerodynamic coefficients are expressed in the body frame,

$$\begin{aligned}
C_l &= (F^l_{uv}\cos\alpha + F^l_{vw}\sin\alpha)\sin\beta\cos\beta + (G^l_{up}\hat{p} \\
&\quad + G^l_{ur}\hat{r})\cos\alpha\cos\beta + F^l_{vq}\sin\beta\hat{q} + (G^l_{wp}\hat{p} + G^l_{wr}\hat{r})\sin\alpha\cos\beta \\
C_m &= (F^m_{uu}\cos^2\alpha + F^m_{uw}\cos\alpha\sin\alpha + F^m_{ww}\sin^2\alpha)\cos^2\beta \\
&\quad + F^m_{vv}\sin^2\beta + (G^m_{uq}\cos\alpha\cos\beta + G^m_{wq}\sin\alpha\cos\beta)\hat{q} \\
&\quad + (G^m_{vr}\hat{r} + G^m_{vp}\hat{p})\sin\beta \\
C_n &= (F^n_{uv}\cos\alpha + F^n_{vw}\sin\alpha)\sin\beta\cos\beta + (G^n_{up}\hat{p} \\
&\quad + G^n_{ur}\hat{r})\cos\alpha\cos\beta + G^n_{vq}\sin\beta\hat{q} + (G^n_{wp}\hat{p} + G^n_{wr}\hat{r})\sin\alpha\cos\beta
\end{aligned} \tag{21}$$

B. Unsteady Aerodynamic Coefficients

This section describes the mathematical model for calculating the unsteady aerodynamic coefficients. The model provides the analytical expressions of the unsteady aerodynamic derivatives in terms of α, β, and M_∞.

As is well known, the unsteady effects are of two kinds [10]; the first effect is directly related to the pressure forces through the Bernoulli theorem, whereas the other is caused by the unsteady motion of the wakes released by the vehicle. The first effect occurs instantaneously and thus depends only on the current state variables, whereas the second one represents the story of the motion of the wakes behind the vehicle from the initial condition until the current time. The present model only considers the first effect, whereas the history of motion is not taken into account. This effect is caused by the term $\Delta p_u = \rho\partial\phi/\partial t$ [10], which appears in the Bernoulli equation in the case of unsteady flow. For assigned velocity variations, such an increment is a function of the time derivatives of the aerodynamic angles and of the flight speed:

$$\Delta p_u = \rho\frac{\partial\phi}{\partial t} \equiv \rho\left(\frac{\partial\phi}{\partial\alpha}\frac{d\alpha}{dt} + \frac{\partial\phi}{\partial\beta}\frac{d\beta}{dt} + \frac{\partial\phi}{\partial V}\dot{V}\right) \tag{22}$$

The effect caused by the time derivatives of the angular velocity is not taken into account. In Eq. (22), the pressure increment is the sum of three terms, the first two of which are due to the time variations of α and β, whereas the last one is caused by the variations of V. For thin vehicles, the last addend is negligible with regard to the first; thus, this is not considered in the present analysis. More conveniently, Δp_u can also be written in terms of the derivatives of the velocity potential $\partial\phi/\partial\hat{u}$, $\partial\phi/\partial\hat{v}$, and $\partial\phi/\partial\hat{w}$:

$$\begin{aligned}
\frac{\Delta p_u}{\rho} &= \frac{\partial\phi}{\partial\hat{u}}\left(-\sin\alpha\cos\beta\,\frac{d\alpha}{dt} - \cos\alpha\sin\beta\,\frac{d\beta}{dt}\right) + \frac{\partial\phi}{\partial\hat{v}}\cos\beta\,\frac{d\beta}{dt} \\
&\quad + \frac{\partial\phi}{\partial\hat{w}}\left(\cos\alpha\cos\beta\,\frac{d\alpha}{dt} - \sin\alpha\sin\beta\,\frac{d\beta}{dt}\right)
\end{aligned} \tag{23}$$

This increment causes aerodynamic force and moment, which are obtained by integrating Δp_u on S_w. Therefore, the unsteady increment of each aerodynamic coefficient varies linearly with $d\alpha/dt$ and $d\beta/dt$, resulting in

$$\begin{aligned}
\Delta C_i &= (A^i_1\sin\alpha + A^i_2\cos\alpha)\cos\beta\dot{\alpha} + (B^i_1\cos\alpha\sin\beta \\
&\quad + B^i_2\cos\beta + B^i_3\sin\alpha\sin\beta)\dot{\beta}
\end{aligned} \tag{24}$$

where A^i_h and B^i_h ($i = D, S, L, l, m$, and n) are opportune surface integrals over S_w of $\partial\phi/\partial\hat{u}$, $\partial\phi/\partial\hat{v}$, and $\partial\phi/\partial\hat{w}$. These integrals are functions of M_∞ and are supposed to be described by expressions such as Eq. (16). The quantities $\dot{\alpha}$ and $\dot{\beta}$ are the dimensionless time derivatives of the aerodynamic angles, which are defined as

$$\dot{\alpha} = \frac{d\alpha}{dt}\frac{L}{V}, \qquad \dot{\beta} = \frac{d\beta}{dt}\frac{L}{V} \tag{25}$$

Thus, the unsteady derivatives of the aerodynamic coefficients are

$$\begin{aligned}
\frac{\partial C_i}{\partial\dot{\alpha}} &= (A^i_1\sin\alpha + A^i_2\cos\alpha)\cos\beta \\
\frac{\partial C_i}{\partial\dot{\beta}} &= B^i_1\cos\alpha\sin\beta + B^i_2\cos\beta + B^i_3\sin\alpha\sin\beta
\end{aligned} \tag{26}$$

Because (x, z) is the vehicle symmetry plane, the derivatives with respect to $\dot{\alpha}$ of the lateral-directional coefficients are identically equal to zero, whereas the derivatives of the longitudinal coefficients depend on α and β. Force and moment coefficients are expressed here in the wind axes. For the $\dot{\alpha}$ derivatives, one obtains

$$\begin{aligned}
\frac{\partial C_D}{\partial\dot{\alpha}} &= (A^D_1\sin\alpha + A^D_2\cos\alpha)\cos\beta, & \frac{\partial C_S}{\partial\dot{\alpha}} &= 0 \\
\frac{\partial C_L}{\partial\dot{\alpha}} &= (A^L_1\sin\alpha + A^L_2\cos\alpha)\cos\beta & \frac{\partial C_l}{\partial\dot{\alpha}} &= 0 \\
\frac{\partial C_m}{\partial\dot{\alpha}} &= (A^m_1\sin\alpha + A^m_2\cos\alpha)\cos\beta, & \frac{\partial C_n}{\partial\dot{\alpha}} &= 0
\end{aligned} \tag{27}$$

whereas the derivatives with regard to $\dot{\beta}$ are

$$\begin{aligned}
\frac{\partial C_D}{\partial\dot{\beta}} &= (B^D_1\cos\alpha + B^D_3\sin\alpha)\sin\beta, & \frac{\partial C_S}{\partial\dot{\beta}} &= B^S_2\cos\beta \\
\frac{\partial C_L}{\partial\dot{\beta}} &= (B^L_1\cos\alpha + B^L_3\sin\alpha)\sin\beta & \frac{\partial C_l}{\partial\dot{\beta}} &= B^l_2\cos\beta \\
\frac{\partial C_m}{\partial\dot{\beta}} &= (B^m_1\cos\alpha + B^m_3\sin\alpha)\sin\beta, & \frac{\partial C_n}{\partial\dot{\beta}} &= B^n_2\cos\beta
\end{aligned} \tag{28}$$

C. Effect of the Controls

This section deals with the effect of the controls on the aerodynamic coefficients. The longitudinal aerodynamic coefficients are first considered. The rotation of the elevator causes a modification in the vehicle geometry, which in turn determines a variation of the aerodynamic force and moment coefficients. For $\delta_e \neq 0$, the aerodynamic coefficients are also described by expressions of the kind in Eqs. (20) and (21) because the latter are applied to a vehicle of a different shape due to $\delta_e \neq 0$. Thus, it is reasonable that the increment of the aerodynamic coefficient caused by δ_e is expressed by

$$\Delta C(M_\infty, \delta_e) = \mathcal{F}_{e1}(M_\infty)\delta_e + \mathcal{F}_{e2}(M_\infty)\delta_e\alpha + \mathcal{F}_{e3}(M_\infty)\delta^n_e \tag{29}$$

In Eq. (29), the first and the second terms represent, respectively, the linear effect of the control and the combined effect of α and δ_e,

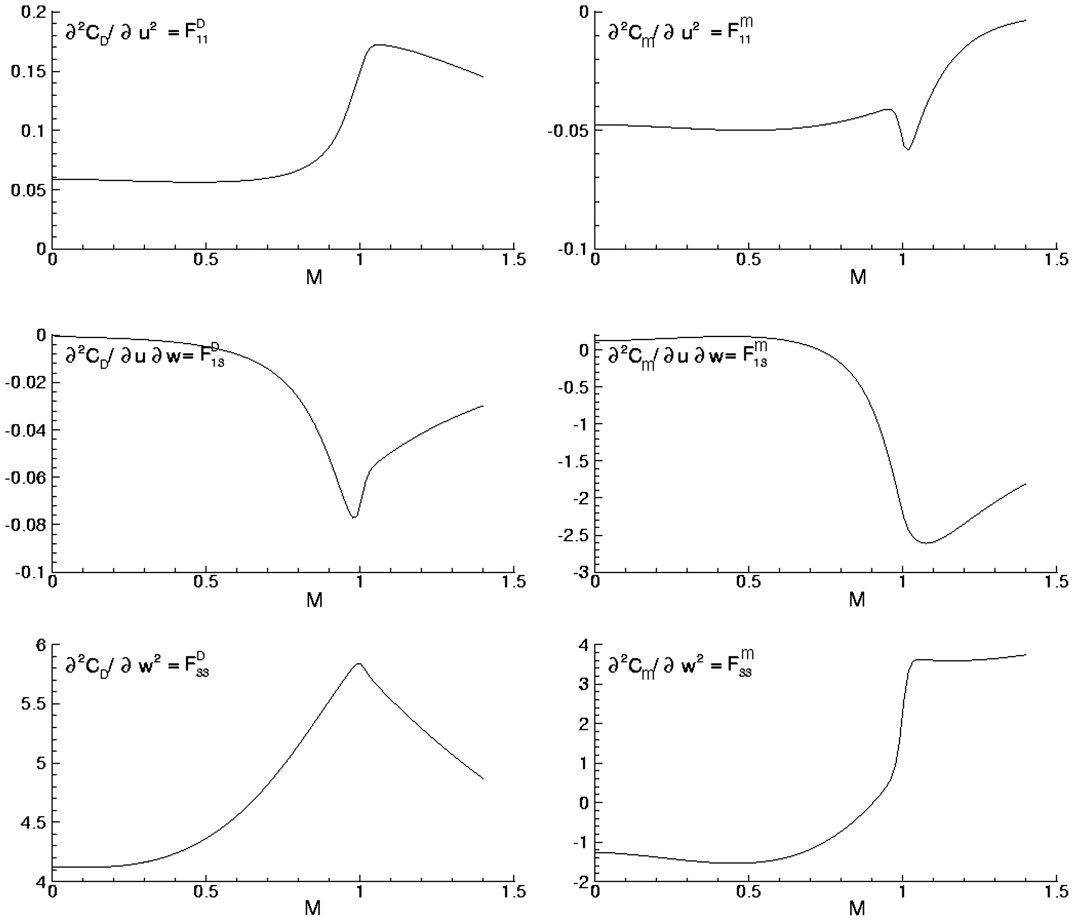

Fig. 5 Static characteristic functions for C_D and C_m.

whereas the third addend is the nonlinear term, for which the exponent n varies (depending on the coefficient). Specifically, it is assumed that $n = 2$ for C_D, whereas $n = 3$ for C_L and C_m. The functions $\mathcal{F}_{e1}(M_\infty)$, $\mathcal{F}_{e2}(M_\infty)$, and $\mathcal{F}_{e3}(M_\infty)$, called (here) the elevator characteristic functions, correspond to surface integrals over S_w, which can be obtained as the difference between the aerodynamic coefficients at $\delta_e \neq 0$ and those for $\delta_e = 0$. These integrals are functions of M_∞, for which the expressions are assumed to be expressed by Eq. (16). The effects of the elevator on the lateral aerodynamic coefficients, which can occur for $\beta \neq 0$, are not considered in the present analysis.

The effects of the ailerons and of the rudders on the lateral-directional aerodynamic coefficients are now described. Again, the rotation δ_a or δ_r determines the variations of the aerodynamic coefficients, for which the value can be obtained as the difference between the aerodynamic coefficients at $\delta_r \neq 0$ ($\delta_a \neq 0$) and those for $\delta_r = 0$ ($\delta_r \neq 0$). These increments are supposed to be expressed by

$$\Delta C(M_\infty, \delta_i) = \mathcal{F}_{i1}(M_\infty)\delta_i + \mathcal{F}_{i2}(M_\infty)\delta_i\alpha + \mathcal{F}_{i3}(M_\infty)\delta_i^2 \qquad (i = a, r) \tag{30}$$

where $\mathcal{F}_{ak}$ and $\mathcal{F}_{rk}$ are called (here) ailerons and rudder characteristic functions, respectively. These are proper surface integrals over S_w, which are functions of M_∞ and for which the analytical structure is supposed to be described by Eq. (16). In Eqs. (30), the first, second, and third terms represent, respectively, the linear control derivative, the simultaneous effects of the angle of attack, and the control and nonlinear contribution of the control.

In conclusion, the aerodynamic coefficients are computed as summations of steady and unsteady contributions plus the effect of the controls. Thus, the force coefficients in wind axes and the moment coefficients in the body frame are both expressed as

$$C_k = (C_k)_s + \Delta(C_k)_u + \Delta(C_k)_c, \qquad k = (D, S, L, l, m, n) \tag{31}$$

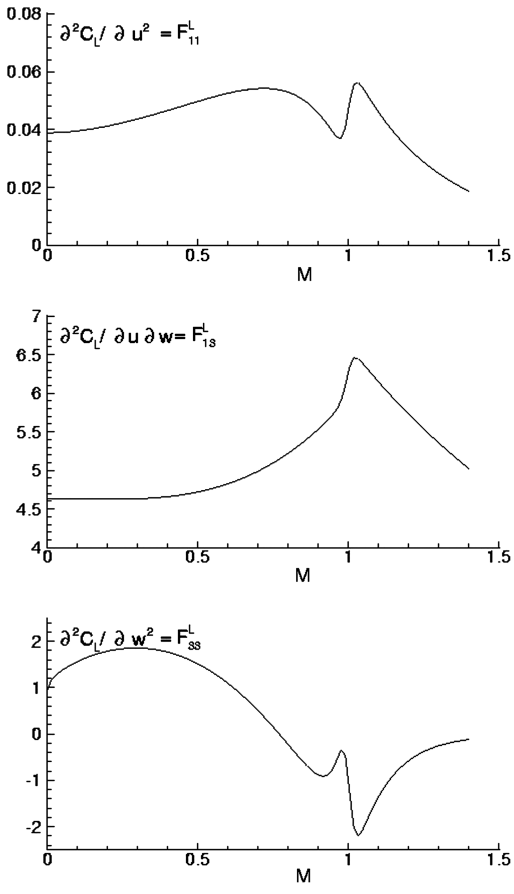

Fig. 6 Static characteristic functions for C_L.

where $(C_k)_s$ and $\Delta(C_k)_u$ indicate the steady and the unsteady parts of the aerodynamic coefficients following Eqs. (20), (21), and (24), respectively, whereas $\Delta(C_k)_c$ denotes the part due to the controls [see Eqs. (29) and (30)]. The gains of each addendum (i.e., F^k_{ij}, G^k_{ih}, A^k_o, B^k_t, F^k_{et}, F^k_{at}, F^k_{rt}, with $i, j = (u, v, w)$; $h = (p, q, r)$; $o = 1, 2$; and $t = 1, 2, 3$) are expressed through Eq. (16), and each gain contains a vector of free model parameters $\theta^k_l \equiv (F_0, m, \epsilon, h_1, h_2, \xi, F_{sup}, g_1, y_1, g_2, y_2)$, with $l = [1, \ldots, Q(k)]$ being $Q(k)$ (the total number of addendum for coefficient k).

IV. Identification Procedure

System identification allows estimating of the values of the free model parameters present in the proposed model. The identification procedure is composed of two steps; the first one is performed before flight, using the information provided by the preflight CIRA-ADB, whereas the second step is carried out after the mission in the postflight data analysis. In the last step, a subset of the free model parameters, selected by means of sensitivity analysis, is estimated in order to update the nominal values and reduce the related uncertainty level.

A. Preflight Identification

The preflight identification of the model-free parameters is carried out through a minimum square method, which for each aerodynamic coefficient, is applied to the following optimization problem:

$$\min_{\boldsymbol{\theta} i} J_i = \min_{\boldsymbol{\theta} i} \sum_{k=1}^{M} [(C^i_k)_{\mathrm{CIRA}} - C^i_k]^2, \qquad i = (D, S, L, l, m, n) \quad (32)$$

where C^i_k and $(C^i_k)_{\mathrm{CIRA}}$ are the aerodynamic coefficients calculated in M points of the flight envelope, with the proposed model and the CIRA-ADB, respectively. J_i is the goal function, defined for each aerodynamic coefficient, for which the arguments are the free parameters $\boldsymbol{\theta}^i \equiv (\theta^i_1, \theta^i_2, \ldots, \theta^i_{Q(k)})$ with the generic θ^i_l composed of parameters appearing in Eq. (16). To obtain the combined effects of the variables α, β, p, q, r, and those of the controls, the coefficients $(C^i_k)_{\mathrm{CIRA}}$ are calculated in a wide range of variation of these variables. This procedure calculates all the free parameters of the model that is all the elements of the vector $\boldsymbol{\theta} = (\boldsymbol{\theta}^D, \boldsymbol{\theta}^S, \boldsymbol{\theta}^L, \boldsymbol{\theta}^l, \boldsymbol{\theta}^m, \boldsymbol{\theta}^n)$. Validation of the identified model can be performed, comparing the aerodynamic coefficients calculated by the proposed model and the CIRA-ADB.

B. Postflight Identification

After mission execution, measured flight data are used to perform system identification, for which the main aim is a refinement of the values identified in preflight for some of the free parameters. First, the subset of parameters to be estimated from the flight data must be

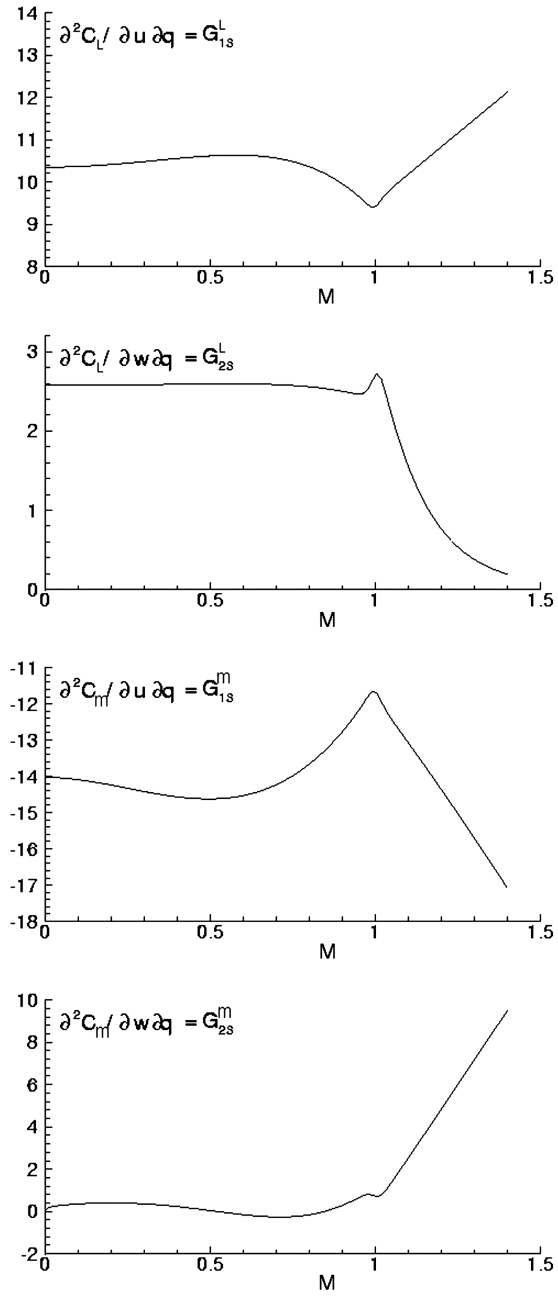

Fig. 7 Rotational characteristic functions for C_L and C_m.

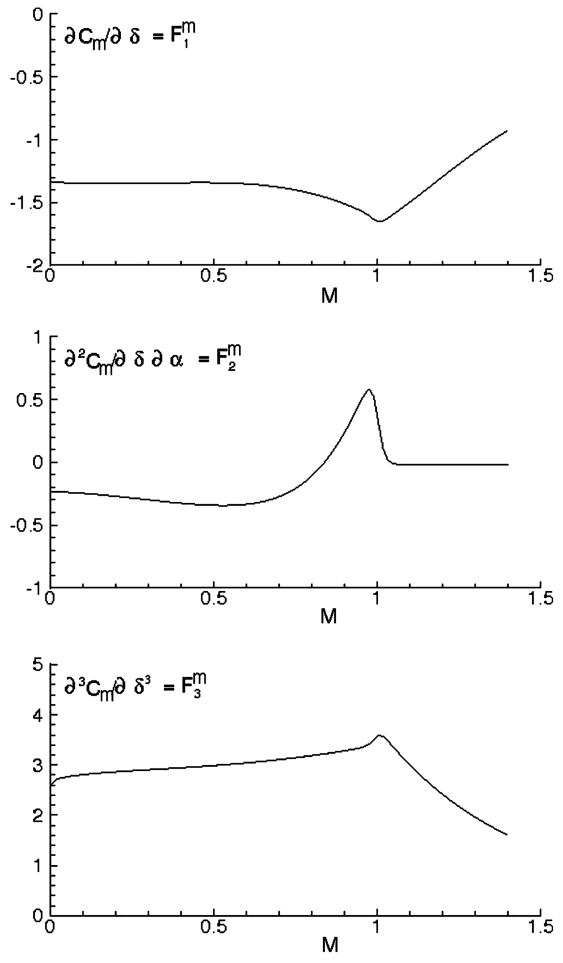

Fig. 8 Elevator derivatives for C_m.

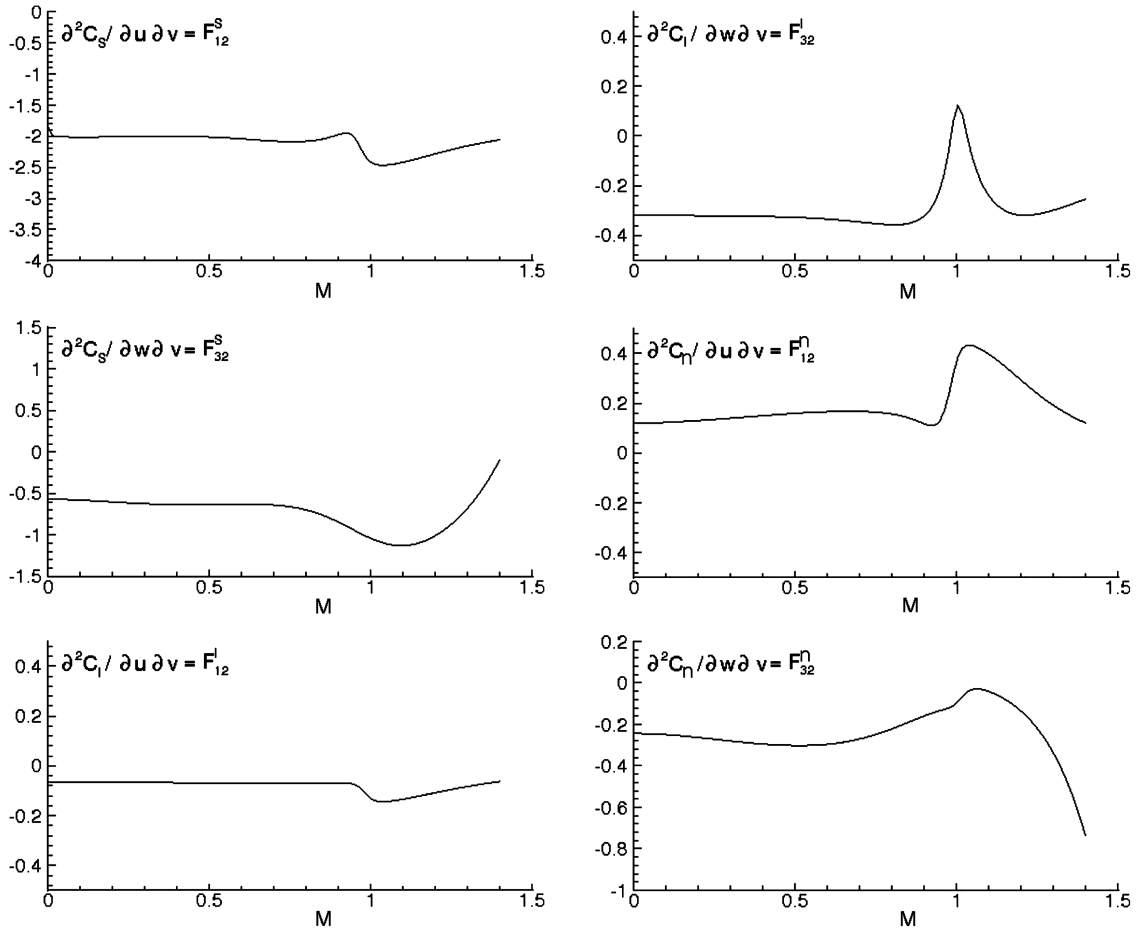

Fig. 9 Static characteristic functions for C_S, C_l, and C_n.

selected. The selection is carried out through an identifiability analysis based on the Cramer–Rao bounds (CRB). The CRB related to the generic parameter $\theta_k \in \boldsymbol{\theta}$, denoted as σ_{θ_k}, is computed through [15]:

$$\mathbf{P} = \left[\sum_{k=1}^{N}\left(\frac{\partial \mathbf{y}(t_k)}{\partial \boldsymbol{\theta}}\right)^T \mathbf{R}^{-1}\left(\frac{\partial \mathbf{y}(t_k)}{\partial \boldsymbol{\theta}}\right)\right] \tag{33}$$

$$\sigma_{\theta_k} = \sqrt{p_{kk}} \tag{34}$$

where $\mathbf{y}$ is the output vector of the system to be identified, gathered in N time instants, which are denoted as t_i. $\mathbf{P}$ represents the error covariance matrix, and p_{kk} is the kth element on the main diagonal of $\mathbf{P}$. The CRB indicate the theoretically maximum achievable accuracy of the estimates and can be considered as a measurement of the sensitivity of system outputs with regard to parameter variations. If the CRB associated to a parameter is bigger than a suitable threshold, the parameter cannot be identified, because its variation has no relevant effect on system outputs (i.e., on flight measurements). After the selection of the parameters to be estimated, their identification is carried out in the framework of a two-step strategy [16], first estimating the vehicle state vector, global aerodynamic coefficients, and some atmospheric properties, then updating the identifiable parameters of the aerodynamic model. Both estimation steps are formulated as nonlinear filtering problems and solved using the unscented Kalman filter. Moreover, the exploitation of all the available a priori information for the stochastic characterization of the filter models and sensors noises, and a rigorous management of all the uncertainties involved in the system identification process, allow us to obtain reliable figures of estimation accuracy. The postflight identification methodology, described in detail in [17], allows a twofold validation of the estimated parameters. First, flight measurements are provided as input to the updated aerodynamic model, and the computed global aerodynamic coefficients are compared with their actual values, estimated in the first estimation step. Second, the updated aerodynamic model is included in a detailed simulation framework, developed to reproduce the flight mission in open loop (without the use of the control system). Flight measurements of the deflection of aerodynamic effectors, deputed to control the vehicle, are used as input to the simulator, which provides output-simulated values of all the other flight measurements. Then, actual flight measurements are compared with the simulated ones in order to evaluate the goodness of the fitting.

V. Results and Discussions

A. Preflight Identification

In the identification procedure, the model-free parameters of the longitudinal aerodynamics are first calculated, whereas in the successive step, the effects on the aerodynamic coefficients of the lateral variables β, p, and r, and of the lateral-directional controls δ_a and δ_r, are analyzed.

1. Identification of the Free Parameters: Longitudinal Coefficients

To calculate the longitudinal aerodynamic coefficients, several data are generated by CIRA-ADB. These data represent diverse situations calculated for $\beta = p = q = r = 0$, varying M_∞ and α.

Figure 5 shows the characteristic functions vs M_∞ for C_D and C_m. According to Eq. (18), $1/2\partial^2 C_D/\partial\hat{u}^2 \equiv C_D(\alpha = 0)$ shows the typical variations of the minimum drag coefficient with M_∞, whereas $\partial^2 C_D/\partial\hat{u}\partial\hat{w} \equiv \partial C_D/\partial\alpha(\alpha = 0)$ is negligible for small M_∞ and at a higher Mach number. The compressibility determines a negative value for this derivative.

The derivative $\partial^2 C_D/\partial\hat{w}^2 \equiv \partial^2 C_D/\partial\alpha^2$, due to the induced drag and the part of the wave drag (which depends on α), can be significant for $M > 0.5$ when α is high enough. This is partially responsible for the diminishing of the drag divergence Mach number as α increases.

Figure 5 also gives the derivatives of C_m in terms of M_∞. According to the linear expansion of C_m, $\partial^2 C_m/\partial\hat{u}^2$ corresponds to $C_m(\alpha = 0)$. This derivative is negative in all the situations, and this implies that the vehicle develops a negative pitching moment at small angles of attack. The derivative $\partial^2 C_m/\partial\hat{u}\partial\hat{w}$ identifies $C_{m\alpha}(\alpha = 0)$, which is just positive in the subsonic regime, thus the vehicle is statically unstable and exhibits quite small variations of $C_{m\alpha}$ with M_∞ until it reaches strongly negative values. This is the typical behavior caused by the backward displacements of the aerodynamic center as M_∞ increases. For $M_\infty > 1$, the characteristic variations of the pitching moment in the supersonic regime are observed. The quantity $\partial^2 C_m/\partial\hat{w}^2$ represents the nonlinear variations of $C_m(\alpha)$, which, according to the theory, are due to the vehicle thickness and to the vorticity developed by the leading edge and forebody.

As far as C_L is concerned (see Fig. 6), the derivative $\partial^2 C_L/\partial\hat{u}^2 \equiv C_L\ (\alpha = 0)$ exhibits quite small variations, and this corresponds to the small changing in the zero lift angle of attack as M_∞ changes, whereas the variations of $\partial^2 C_L/\partial\hat{u}\partial\hat{w} \equiv C_{L\alpha}\ (\alpha = 0)$ are almost in line with the theoretical topics of the compressible aerodynamics. As $C_{L\alpha} \approx 4.6$ for $M_\infty \to 0$, it increases with M_∞, reaching its maximum value at $M_\infty \approx 1$, and thereafter decreases according to the laws of the supersonic aerodynamics. The quantity $\partial^2 C_L/\partial\hat{w}^2$ represents the nonlinear part of $C_L(\alpha)$, which is partially caused by the vorticity due to the wing leading edge and the vehicle forebody. This is positive for $M_\infty < 1$ and is in quite good agreement with the Polhamus theory (see [18] and the references therein), which gives $\partial^2 C_L/\partial\hat{w}^2 \approx 1/3$ for $M_\infty < 1$.

Next, the effect of the angular velocity is taken into account with Eqs. (20) and (21). Because these equations are linear with regard to $\boldsymbol{\omega}$, these identify the rotational derivatives, which depend on α, β, and M_∞. To determine the pitch rate effect, various data are calculated with CIRA-ADB, assuming $\hat{q} = 0.01$ and 0.02. The increment of the aerodynamic coefficients due to the spin rate is calculated as the difference between the data obtained for $q \neq 0$ and those calculated with $q = 0$. Again, the free parameters of the model are identified through the aforementioned minimum square method.

Figure 7 illustrates the rotational characteristic functions [see Eq. (15)] of C_L and C_m. According to Eq. (19), $\partial^2 C_L/\partial\hat{u}\partial\hat{q} \equiv \partial C_L/\partial\hat{q}\ (\alpha = 0)$, whereas $\partial^2 C_L/\partial\hat{w}\partial\hat{q}$ describes the contribution due to the angle of attack. From these diagrams, it is apparent that the main contribution to $\partial C_L/\partial\hat{q}$ is given by $\partial^2 C_L/\partial\hat{u}\partial\hat{q}$, which exhibits its minimum for $M_\infty \simeq 1$, whereas the other term, responsible for the variations with α, produces minor effects. The average of $\partial C_L/\partial\hat{q}$ is in agreement with the data reported in [4]. The figure also shows the variations of $\partial^2 C_m/\partial\hat{u}\partial\hat{q}$ and $\partial^2 C_m/\partial\hat{w}\partial\hat{q}$ in terms of M_∞. The derivative $\partial^2 C_m/\partial\hat{u}\partial\hat{q} \equiv \partial C_m/\partial\hat{q}$ expresses the damping derivative at $\alpha = 0$, whereas $\partial^2 C_m/\partial\hat{w}\partial\hat{q}$ describes the variations with the angle of attack. Both the diagrams show quite flat curves in the subsonic regime and monotonic laws for $M_\infty > 1$. For what concerns the drag coefficients, according to CIRA-ADB, it is not influenced by the pitch rate.

Finally, the effect of the elevator is analyzed in Fig. 8, for which the control derivatives of C_m are given in terms of M_∞. All the derivatives with regard to δ_e exhibit small variations in the subsonic region, for which, in the transonic and supersonic regimes, more sizable variations are observed. The cross derivatives, $\partial^2/\partial\alpha\partial\delta_e$, exhibit more pronounced variations in all of the regimes.

In all of the situations, the proposed model adequately describes the variations of the aerodynamic coefficients with a maximum error with regard to a CIRA-ADB smaller than 4%.

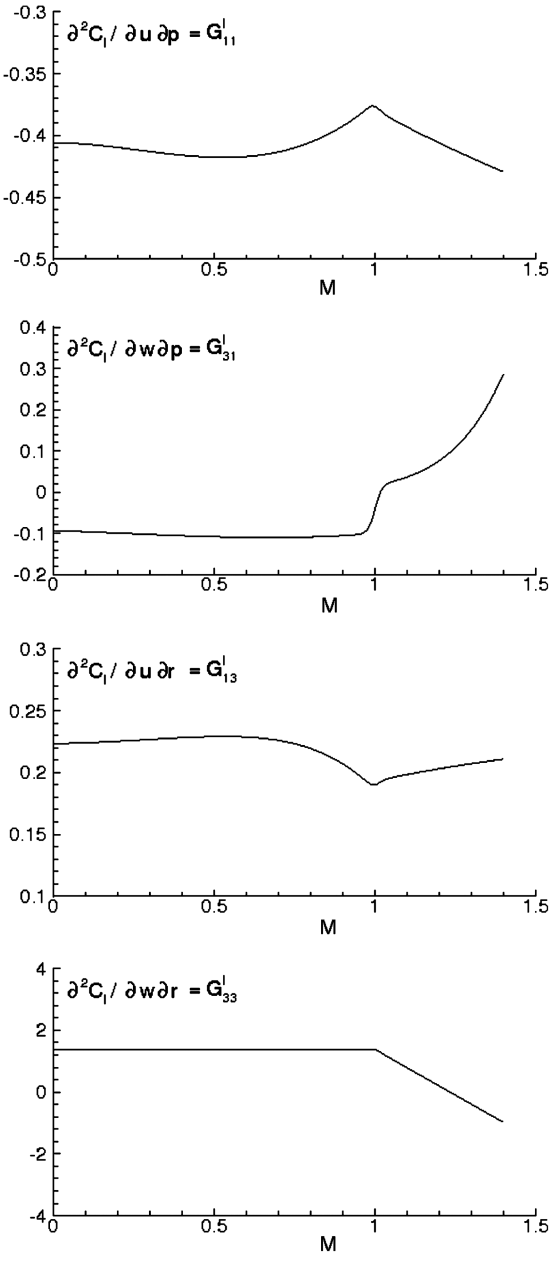

Fig. 10 Rotational characteristic functions for C_l.

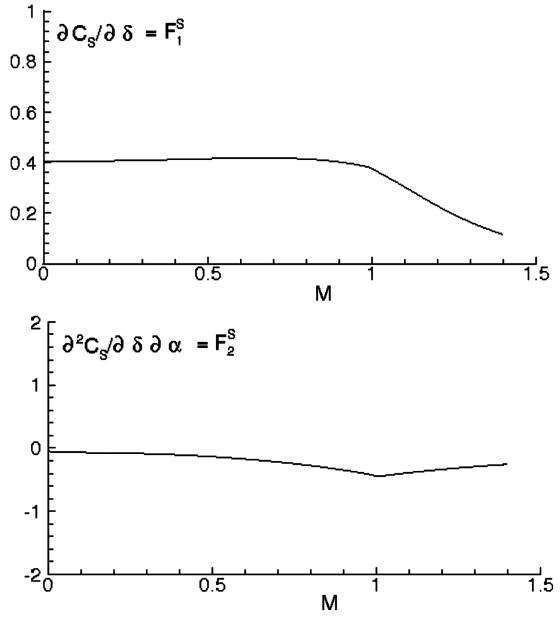

Fig. 11 Aileron derivatives for C_S.

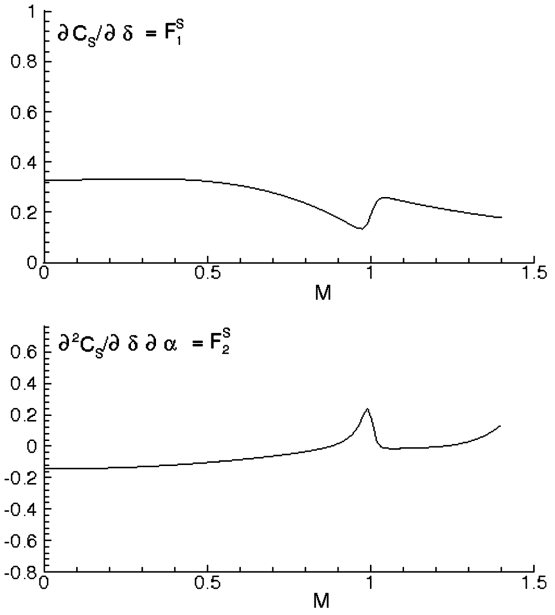

Fig. 12 Rudder derivatives for C_S.

2. Identification of the Free Parameters: Lateral-Directional Coefficients

Now, we analyze the effects of the lateral variables β, $\hat{p}$, and $\hat{r}$, and of the lateral-directional controls δ_a and δ_r, on the aerodynamic coefficients. First, to obtain the static aerodynamic coefficients, three sets of data are generated using CIRA-ADB. These sets of data are obtained for $\beta = 2, 4$, and 6 deg, $\boldsymbol{\omega} = 0$, where α and M_∞ assume the same values of the previous data concerning the longitudinal aerodynamics. These data are processed with the minimum square method, and the free parameters of each aerodynamic coefficient are calculated.

Figure 9 shows the influence of the sideslip angle on the aerodynamic side force and on the moment coefficients C_l and C_n. In particular, the figure depicts the derivative $\partial C_S/\partial\beta$ and gives the variations of the dihedral effect and the yaw stiffness in the function of M_∞.

The diagrams of Fig. 10 show the characteristic rotational functions of C_l, which correspond to the rotational derivatives associated to the coefficients. These are practically constant until $M_\infty = 1$ and thereafter exhibit variations with M_∞, which agrees with [4].

Figures 11 and 12 show, respectively, the effects of δ_a and of δ_r on the side-force coefficient, which are calculated through Eqs. (30).

Table 1 Estimated aerodynamic parameters

Parameter	Preflight value	Estimated value	Estimation standard deviation	Reference aerodynamic derivative
F^D_{10}	0.059	0.048	0.001	C_{D0}
$F^D_{1\,\mathrm{sup}}$	−1.29	−1.18	0.005	C_{D0}
F^D_{20}	−6e − 5	2e − 4	1e − 5	$C_{D\alpha}$
$F^D_{2\,\mathrm{sup}}$	−0.13	−0.30	0.02	$C_{D\alpha}$
F^D_{30}	4.12	3.11	0.05	$C_{D\alpha^2}$
$F^D_{3\,\mathrm{sup}}$	4.81	6.32	0.11	$C_{D\alpha^2}$
F^L_{10}	0.04	5e − 4	0.0001	C_{L0}
$F^L_{1\,\mathrm{sup}}$	−0.32	0.19	0.003	C_{L0}
F^L_{20}	4.41	4.04	0.001	$C_{L\alpha}$
$F^L_{2\,\mathrm{sup}}$	8.14	7.97	0.015	$C_{L\alpha}$
F^L_{90}	1.59	1.23	0.001	$C_{L\delta_e}$
$F^L_{9\,\mathrm{sup}}$	0.86	0.70	0.006	$C_{L\delta_e}$
$F^m_{1\,\mathrm{sup}}$	−0.06	0.004	0.007	C_{m0}
$F^m_{2\,\mathrm{sup}}$	−0.22	−0.17	0.01	$C_{m\alpha}$
$F^m_{5\,\mathrm{sup}}$	−4.15	−6.79	4.56	C_{mq}
$F^m_{9\,\mathrm{sup}}$	−1.49	−0.98	0.07	$C_{m\delta_e}$

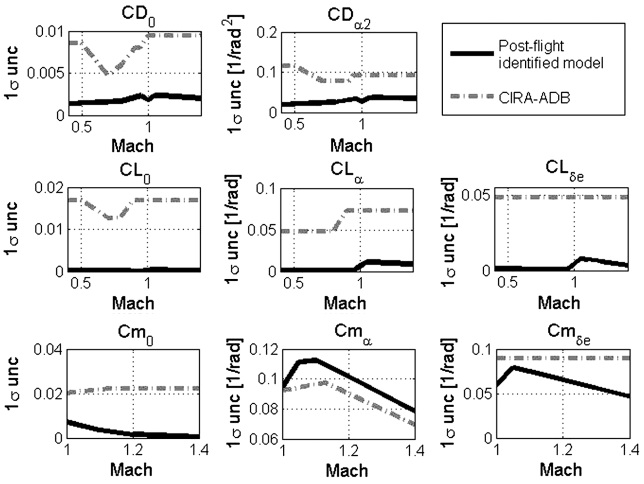

Fig. 13 1σ uncertainties of the main derivatives vs the Mach number for the CIRA-ADB and the postflight-identified aerodynamic model.

Because of the vehicle symmetry, at $\beta = 0$, the longitudinal coefficients (C_D, C_L, and C_m) are even functions of δ_a and δ_r, whereas C_S, C_l, and C_n result in odd functions of these controls.

Once the model-free parameters are identified, the maximum error with regard to CIRA-ADB is less than 3% for each lateral-directional aerodynamic coefficient.

B. Postflight Identification

The analysis of DTFT_1 data in postflight allows only the update of some longitudinal parameters of the analytical model. Because the flight trajectory is basically longitudinal, the excitation of lateral-directional dynamics is very poor. Through the sensitivity analysis based on the CRB, the parameters listed in Table 1 were selected for identification. The flight measurements are divided into two intervals. The first one, from 17 through 36 s flight time, is used for estimating the subsonic parameters, whereas the measurements from 38 to 44 s of flight allow the estimation of the supersonic ones. Each longitudinal coefficient is analyzed independently, and the parameter estimation in subsonic and supersonic regimes is carried out independently. In Table 1, preflight and postflight estimated values of the parameters are shown together with the estimated standard deviations of postflight estimations. As shown in the last column of the table, the parameters are basically related to zero-order terms and to the aerodynamic derivatives of C_L and C_m with regard to α, q, and

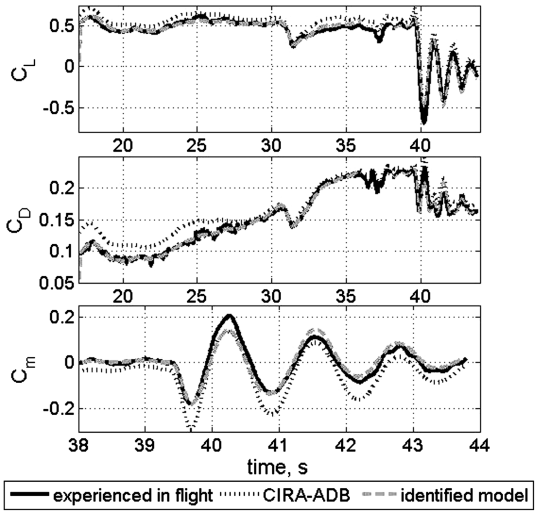

Fig. 14 Comparison between aerodynamic coefficients experienced in flight by the vehicle, computed using the identified model and the CIRA-ADB.

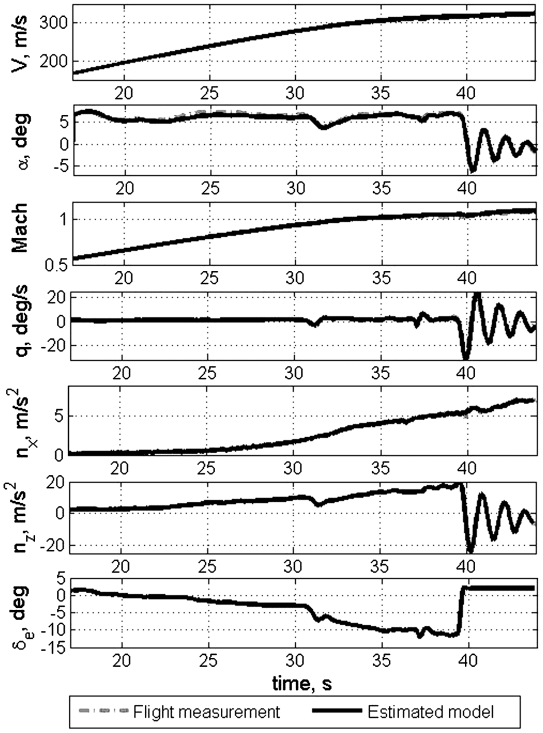

Fig. 15 Time history comparison of flight measurements and estimated model responses.

δ_e, and of C_D with regard to α. Note in the table that significant corrections are calculated for the zero-order components of C_L and C_m and to the derivatives $C_{L\delta_e}$ and $C_{m\delta_e}$, whereas the $C_{L\alpha}$ estimation is very close to its preflight value. All the analytical model parameters not listed in the table are held constant to their preflight values. Following the postflight identification, the uncertainty ranges of the main aerodynamic derivatives for the updated model are, in most cases, significantly reduced with regard to CIRA-ADB as shown in Fig. 13, in which the 1σ uncertainties vs the Mach number are presented. The uncertainties on aerodynamic derivatives for the identified model are computed propagating the uncertainties on aerodynamic parameters through the analytical model. To validate the identified nominal values of the parameters, the aerodynamic coefficients experienced in flight by the vehicle (provided by the first step of the postflight identification procedure [17]) are compared with the analogous coefficients computed using flight measurements and provided by the identified model and the CIRA-ADB. The comparison, presented in Fig. 14, shows the improved capability of the identified model with regard to CIRA-ADB to fit the actual aerodynamics, at least along the trajectory performed during the $DTFT_1$ mission. It is worthy to note that, because identification of pitching moment coefficient has been only carried out in supersonic regime, the aforementioned comparison for such a coefficient is only shown in the time frame from 38 to 44 s of flight time. Furthermore, an open-loop simulation (without control system) is performed using the updated aerodynamic model, and the output is compared with flight measurements. Because the updated model of the pitching moment is not available in the subsonic regime, only in this regime the global coefficient experimented in is flight used to simulate the vehicle aerodynamic behavior. The 6-degrees-of-freedom dynamics of the FTB_1 vehicle and the sensor dynamics are implemented in the simulation model. Inputs to the simulator are the in-flight measurements of elevons and rudder deflections. The obtained results are shown in Fig. 15, in which very good agreement between flight data and simulation output is apparent (the trajectories are almost indistinguishable). It is worthy of remark that if the same verification is performed with the CIRA-ADB, the simulation results show an unsteady behavior of the vehicle, which is totally in disagreement with the actual flight measurements.

VI. Conclusions

In this paper, a novel structured aerodynamic model used for identification of the aerodynamic coefficients of a lifting body in subsonic, transonic, and supersonic regimes is presented. The proposed model is based on the general properties of the continuity equation in the von Kármán form, taking into account physical hypothesis about the flow around the vehicle and the simultaneous effects of several variables that characterize the vehicle state. Each aerodynamic coefficient is expressed through analytical relations, which incorporate various free parameters, to be identified from the analysis of flight data. As a major advantage of such a structured model, the parameter values obtained from the analysis of a single trajectory, due to the physical basis of the model, could be extended to a wide region of the flight envelope. This characteristic is relevant, especially if few flight tests specifically aimed at system identification can be performed, as usually happens for a reentry vehicle. The application of the proposed model for the aerodynamic identification from flight data of the $DTFT_1$ vehicle developed by CIRA has shown that it is suitable for an excellent fitting of the actual aerodynamic coefficients experimented in flight by the vehicle. The reliability of the updated model over an expanded flight envelope will be carefully analyzed and assessed when the flight data of the next FTB_1 missions will be available.

Acknowledgments

This work was executed in the framework of the GNC technology Post Flight Analysis project within the CIRA USV National Aerospace Research Program (PRORA-USV) and supported under contract 04/2005. This work was partially supported by the Italian Ministry of University.

References

[1] Lamb, H., "On the Motion of Solids Through a Liquid," *Hydrodynamics*, 6th ed., Dover, New York, 1945, pp. 160–201.

[2] Brauckmann, G. J., "X-34 Vehicle Aerodynamic Characteristics," *Journal of Spacecraft and Rockets*, Vol. 36, No. 2, 1999, pp. 229–239. doi:10.2514/2.3453

[3] Kawato, H., Watanabe, S., Yamamoto, Y., and Fujii, K., "Aerodynamic Performances of Lifting-Body Configurations for a Reentry Vehicle," *Journal of Spacecraft and Rockets*, Vol. 42, No. 2, 2005, pp. 232–239. doi:10.2514/1.2418

[4] Roskam, J., "Airplan Design Part VI: Preliminary Calculation of Aerodynamic Thrust and Power Characteristics," Design Analysis Research Corp., Lawrence, KS, 2000.

[5] Raymer, D. P., *Aircraft Design: A Conceptual Approach*, AIAA Education Series, AIAA, Reston, VA, 1996.

[6] Hildebrand, F. B., *Introduction to Numerical Analysis*, Dover, New York, 1987.

[7] Ferrari, C., and Tricomi, F., *Transonic Aerodynamics*, Academic Press, New York, 1968.

[8] Cole, J. D., and Cook, L. P., *Transonic Aerodynamics*, North–Holland, New York, 1986.

[9] Shapiro, A. H., *The Dynamics and Thermodynamics of Compressible Fluid Flow*, Vol. 1–2, Ronald, New York, 1953.

[10] Ashley, H., and Landahl, M., *Aerodynamics of Wings and Bodies*, 6th ed., Dover, New York, 1965, pp. 29–44.

[11] de Divitiis, N., "Performance and Stability Analysis of a Shrouded-Fan UAV," *Journal of Aircraft*, Vol. 43, No. 3, 2006, pp. 681–691. doi:10.2514/1.16210

[12] Rufolo, G. C., Roncioni, P., Marini, M., Votta, R., and Palazzo, S., "Experimental and Numerical Aerodynamic Data Integration and Aerodatabase Development for the PRORA-USV-FTB_1 Reusable Vehicle," 14th AIAA/AHI Space Planes and Hypersonic Systems and Technologies Conference, AIAA Paper 2006-8031, Nov. 2006.

[13] Pastena, M., Di Donato, M. P., Di Palma, L., Guidotti, G., Pellone, L., Rufolo, G., and Sabatano, R., "PRORA USV1: The First Italian Experimental Vehicle to the Aerospace Plane," AIAA/CIRA 13th International Space Planes and Hypersonic Systems and Technologies Conference, AIAA Paper 2005-3348, May 2005.

[14] Guckenheimer, J., and Holmes, P., *Nonlinear Oscillations, Dynamical Systems, and Bifurcations of Vector Fields*, Springer, New York, 1990.

[15] Jategaonkar, R., *Flight Vehicle System Identification: A Time Domain Methodology*, Progress in Aeronautics and Astronautics, Vol. 216,

AIAA, Reston VA, Aug. 2006.
[16] Hoff, J. C., and Cook, M. V., "Aircraft Parameter Identification Using an Estimation-Before-Modelling Technique," *The Aeronautical Journal*, Vol. 100, No. 997, Aug.–Sept. 1996, pp. 259–268.
[17] Vitale, A., Corraro, F., Bernard, M., and De Matteis, G., "Unscented Kalman Filtering for Identification of a Re-Entry Vehicle in Transonic Regime," *Journal of Aircraft*, Vol. 46, No. 5, 2009, pp. 1649–1659. doi:10.2514/1.42256
[18] McCormick, B. W., *Aerodynamics, Aeronautics, and Flight Mechanics*, Wiley, New York, 1994.

R. Cummings
Associate Editor